UNIVERSITY OF CALIFORNIA SAN DIEGO

Dynamic size distributions and modeling for aggregation of *Alteromonas* sp. 4B03 in peptone culture

A Thesis submitted in partial satisfaction of the requirements
for the degree Master of Science

in

Materials Science and Engineering

by

Yonghan Wu

Committee in charge:

Professor Terence Hwa, Chair
Professor Oleg Shpyrko, Co-Chair
Professor Monica Allen

2022

The Thesis of Yonghan Wu is approved, and it is acceptable in quality and form for publication on microfilm and electronically.

University of California San Diego

2022

TABLE OF CONTENTS

LIST OF FIGURES

ACKNOWLEDGEMENTS

I would like to express my special thanks to my supervisor Terence Hwa and my mentor Jacob Robertson for their help and advice during the course of my MS degree. Prof. Hwa has been very helpful in developing models and provided insightful comments and suggestions in research and life experience. Jacob Robertson has been very helpful all the time in lab and is really influential in shaping my experiment method and analyzing my results. Their guidance has helped me in all the time of research and writing of this thesis.

I would also like to thank Tolga Caglar and Ghita Guessous for their technical support in microscopy and my thesis committees and all the members in Hwa's lab.

Chapter 1 contains unpublished material coauthored with Jacob Robertson and Terence Hwa. Jacob Robertson. The thesis author was the primary author of this chapter.

Chapter 2 in part is currently being prepared for submission for publication of the material. Robertson, Jacob; Wu, Yonghan; Hwa, Terence "Microscopic size distributions and coagulation modeling allow estimation of cellular stickiness in copiotrophic marine bacterium Alteromonas sp. 4B03". The thesis author was the primary researcher and author of this chapter.

ABSTRACT OF THE THESIS

Dynamic size distributions and modeling for aggregation of *Alteromonas* sp. 4B03 in peptone culture

by

Yonghan Wu

Master of Science in Materials Science and Engineering

University of California San Diego, 2022

Professor Terence Hwa, Chair
Professor Oleg Shpyrko, Co-Chair

As a major component of marine snow, bacteria play an important role in the ocean's biological pump. While it has been demonstrated that bacteria effect aggregation of phytoplankton in vitro, the conditions and process of aggregation for marine bacteria remains poorly understood. In this study, we characterized the aggregation behavior of a particle-associated bacterial isolate *Alteromonas* sp 4B03. Based on optical density (OD_{600}) measurement, 4B03 rapidly aggregates

and disaggregates in the first hour after transferred from acetate minimal media to complex media containing peptides. To quantitatively understand 4B03's aggregation process following introduction to peptides, we use confocal microscopy to characterize the temporal development of aggregates size distributions. Growth of aggregate size is confirmed, evident in both the drop of single cell density and an increase in the abundance of larger aggregates. Moreover, a model is built for the initial aggregation process which relates single cell dynamics to motility-based encounter rate and stickiness. The model enables estimation of cellular stickiness values using single cell counts from size distributions and measurements of cellular motility. Simulations of aggregates dynamics that take into account cell replication and single cell detachment from aggregates was done to recapitulated experimental findings. To our knowledge, this work offers the first experimental determination of cellular stickiness values in marine bacteria, which may enable incorporation of this important group of organisms into large-scale oceanographic models of aggregation.

1 INTRODUCTION

1.1 ROLE OF AGGREGATION IN THE CONTEXT OF MARINE ECOLOGY

Phytoplankton, photosynthetic marine microbes, plays an important role in converting CO_2 in atmosphere to organic form---they are responsible for about half of the planet's CO_2 fixation [1]. Coagulation of marine bacteria with phytoplankton and other organic particle can form large sinking aggregates in ocean called marine snow. Since the residence time of organic matter in the ocean increases as it reaches greater depth, marine snow plays a major role in carbon sequestration in ocean [2]. In addition, it can also serve as a nutrient hot spot that provides food source for shrimp, fish, and other zooplankton [3] [4]. While the importance of marine snow in food webs and global carbon sequestration is clear, the initial formation process of marine snow remains poorly understood.

For a long time, phytoplankton has been the sole focus for study about marine snow formation; people made measurements and models on stickiness value of phytoplankton [5] [6]. But it has been shown that in some cases, bacteria are important in aggregation formation [7]. In that study, people cultured phytoplankton with and without a nature occurring community of marine bacteria [7]. They found no aggregation in phytoplankton culture that without bacteria, but with large amounts of aggregation in culture with bacteria [7]. This suggests bacteria not only decomposition of organic particle [8] but also in involved in aggregation process that forms marine snow. It was also shown that interactions between bacteria and diatoms could promote aggregation and thus particle sinking [9]. In addition, several studies by Kiørboe and colleagues rigorously exam particle colonization and dispersal of marine bacteria using agar spheres and found several interesting phenomena. They observed an increased colonization of substrate-enriched spheres compared to unenriched, increase in colonization rate under flow, and faster colonization for

spheres are embedded with diatoms [7] [10] [11]. However, there are many questions remains for bacteria, such as the range of stickiness, conditions that would make bacteria favorable to aggregate/disaggregate, or the mechanisms of aggregation formation. We are interested in these questions and is curious about what we can learn by studying a single strain in depth. We studied the bacterium *Alteromonas* sp. 4B03, a member of a widespread, particle-associated genus that isolated from a particle-colonizing enrichment of marine bacteria [12]. This gives us insight on conditions for aggregation and stickiness value.

1.2 ALTEROMONAS: A WIDE-SPREAD PARTICLE ASSOCIATED GENUS

There are many studies comparing particle-attached and free-living marine bacterial communities in the upper ocean (epipelagic) and mesopelagic [13] [14] [15]. In these studies, class γ-proteobacteria are typically found to be enriched or abundant on particles, among which genus *Alteromonas* is often prevalent in the community profile. Metagenomics data has shown low abundance and particle enriched *Alteromonas* in eastern subtropical Pacific microbial communities [16]. We believe that the prevalence of *Alteromonas* in particles and aggregates motives the further study of aggregation behaviors and dynamics in representatives of this genus.

Studying aggregation of *Alteromonas* will add to our understanding in aggregates formation in ocean. In this study, we measured dynamics of aggregates size distributions of *Alteromonas*. sp. 4B03 and interpreted dynamics size distributions by an aggregation model to determine stickiness value for given conditions.

1.3 GROWTH AND AGGREGATION OF 4B03 IN DIFFERENT NUTRIENT SOURCE

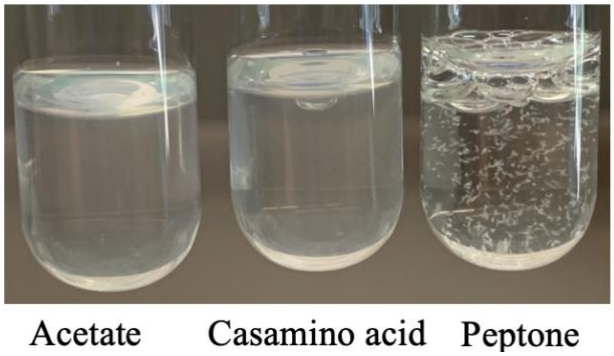

Figure 1. Qualitative observation of growth and aggregation in different carbon source. (credit: Jacob Robertson, PhD student)

When cells being transferred from acetate preculture to batch culture with different carbon source (acetate, casamino acid and peptone), we found that while cells growth planktonically in acetate and casamino acid (cAAs), they aggregate a lot in peptone (Fig. 1). To have a better understanding of aggregation and growth, we need to quantitatively measure cell density and fraction of cells that are aggregated.

$$OD = -\log_{10}\frac{I_1}{I_0}$$

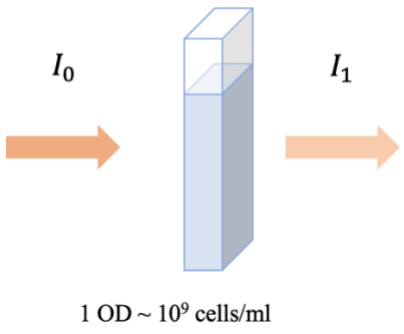

Figure 2. Demonstration for optical density spectrometer

Optical density, obtained by measuring the intensity of incoming light and outgoing light through the liquid culture, is a commonly used way to measure cell density in the culture (Fig. 2). One OD corresponds to approximately 10^9 cells/ml.

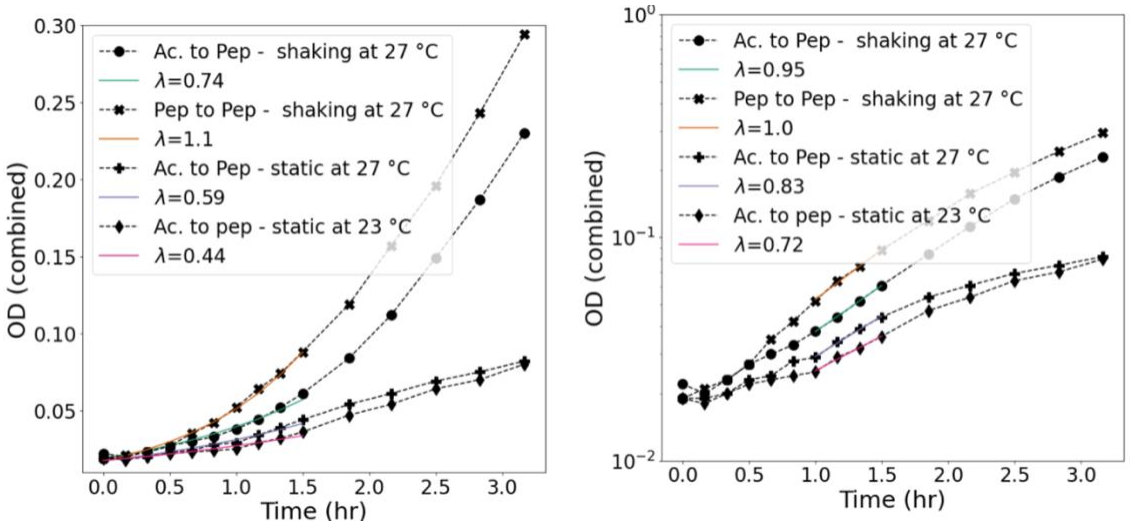

Figure 3. Growth rate measurement in different conditions in peptone 0.25%. Left: Semi-log plot where λ is exponential growth rate; right: linear plot with λ the average growth rate in the first 1.5 h.

Using optical density spectrometer, we measured the growth of Alteromonas. sp 4B03 under shaking or static conditions at room temperature (23 °C) and at typical temperature for marine bacteria (27 °C). Peptone was used to mimic real environment. When carbon source was shifted from acetate to peptone, 4B03 shows a ~30 min lag time. Exponential growth rate is around 1 hr^{-1} for shaking conditions and lower in static condition. Our experiments are mostly done in the first 1.5 h after transferred to new media, average growth rates of first 1.5 h are also fitted (Fig. 3 left), which is used latter in simulations.

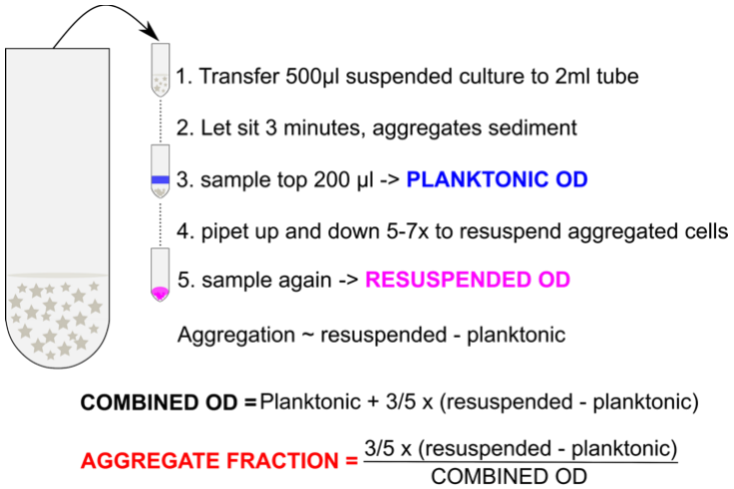

Figure 4. An OD based method to measure growth and aggregation in bacterial cultures: (a) using sedimentation of aggregates, obtaining total/combined OD and aggregated fraction.

Taking advantage of the fact that aggregates sediment in the absence of shaking, a PhD student in our lab Jacob Robertson have made extensive use of an optical density-based method for simultaneously tracking the growth and aggregation of a culture (Fig 4). Using this method we can simultaneous measure the total OD (~total bacterial biomass) and the fraction of biomass that is in sinking aggregates (aggregation fraction). This method is used to describe aggregation dynamics in aggregation conditions below.

If not specifically stated, the preculture condition is exponential growing cells in MBL minimal medium with acetate as the sole carbon source, which is a planktonic growth condition for 4B03.

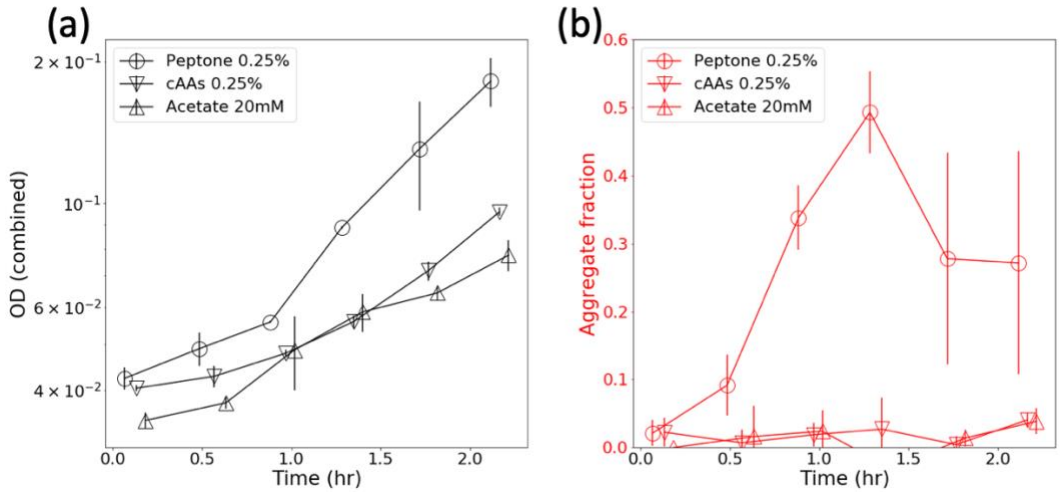

Figure 5. Growth and aggregation of 4B03 immediately following transfer from acetate to peptide or amino acid nutrients. Error bars are 2*S.D. from 2 technical replicates. (credit: Jacob Robertson, PhD student)

When cells growing planktonically in MBL-acetate are transferred to MBL peptone, aggregation is visually detectable within 30 minutes and a peak aggregated fraction >0.4 is reached within 1-1.5 hours (Fig. 5b), whereas transfer to acetate or casamino acids leads to no detectable aggregation (Fig 5b).

Following the rapid aggregation in peptone, the aggregation fraction reduces immediately after ~1.5 hour. This initial aggregation peak raises our interests and become the focus for our study. Next, we would like to know how peptone concentration would affect the aggregation.

Acknowledgements

Chapter 1 contains unpublished material coauthored with Jacob Robertson and Terence Hwa. Jacob Robertson. The thesis author was the primary author of this chapter.

2 AGGREGATION BEHAVIOR IN PEPTONE

2.1 INTRODUCTION

To characterize 4B03's aggregation and disaggregation behavior in peptone, we varied the concentration of peptone to which 4B03 is transferred. Different concentration (0.01%-1%w/v) leads to similar growth patterns (Fig 6a) but a range of aggregation responses (Fig 6b). At all concentrations, an initial peak of aggregation was observed within the first 1h. The initial aggregation peak increased monotonically with the peptone concentration from 0.1% to 1%. Moreover, at all concentrations, the aggregate fraction drops after 2h. These data further confirmed that 4B03 has an exceptionally strong initial response to peptide exposure, followed by a less aggregating period.

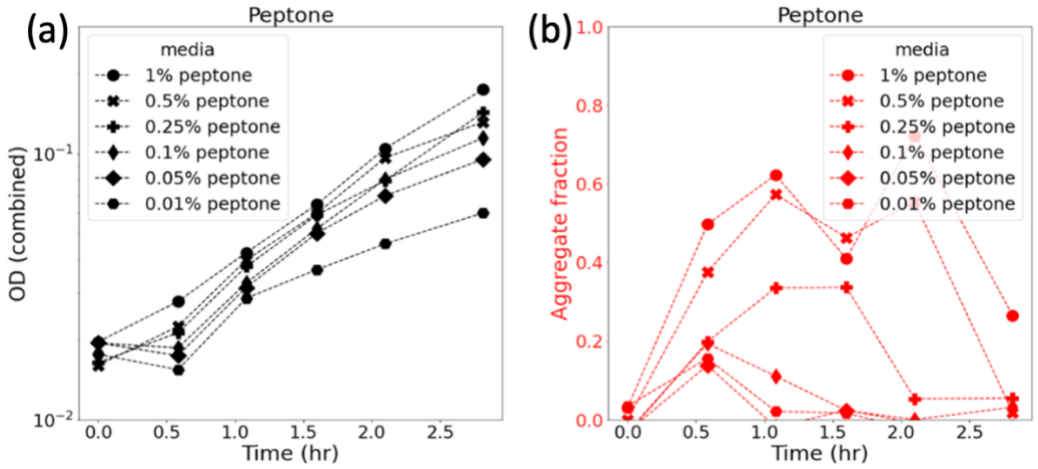

Figure 6. Initial aggregation response of 4B03 transferred from acetate to varying concentrations of peptone at initial OD 0.02.

These OD based experiments may provide us with valuable information about the nature of the aggregation dynamics. When cell density is fixed, we observed a higher and wider aggregation peak with increasing peptone concentration. This suggests that peptone could trigger either the motility or the cell stickiness to increase, making cells aggregates faster and stay longer in aggregated phase. We turned to microscopic observations of cellular aggregation and motility following introduction of peptone to further investigate these dynamics.

2.2 RESULT AND DISCUSSIONS

2.2.1 SIZE DISTRIBUTION OVER TIME

To quantitatively understand the aggregation dynamics, we want to observe how single aggregates form starting from a culture of single cell. We develop a microscopic way to measure aggregates size distributions (section 2.4). Figure 7 depicts the size distributions of aggregates and single cells in the first 80 min after transferred to 0.5% peptone culture. The aggregate size is reported in 'biovolume' which is obtained by calibrating with aggregates size using confocal microscope, and is proportional to number of cells. At 0 min, the cells were just transferred and

1.5 μm filtered to leave mostly single cells. A clear peak of single cell can be seen at ~ 0.12 μm^3, and it drops as a power law with biovolume, observable up to aggregate of size~20 for the sampled culture. The width of the peak could be caused by some uneven dyed cells or out-off focus cells. At 20 min, the single cell peak drop by around 2-fold and a shoulder-like structure is found in the distribution for biovolume~ 0.25-1 μm^3, corresponding to aggregates with 2 to 8 cells. For biovolume > 1 μm^3 the same power law tail is remained. The single cell peaks drop by around 6-fold from 0 min to 80 min but remains distinct in every distribution. Moreover, the peak position itself increase 2-fold to 0.25 μm^3 during this time, reflecting the increase in cell size after transfer form slow growth in acetate to fast growth in peptone media.

On the higher biovolume side, we observed that the power law trend is maintained and continued to expand at a similar rate, with the size of larger aggregates doubling every 12 min. Total biovolume, which gives information about total cell growth, can also be obtained from the biovolume distribution. As illustrated in Fig. 7 (b) and (c), total biovolume increase by ~2-fold in 80 min while average cluster size increased by ~10-fold. This suggests that cell doubling inside cluster cannot be the sole reason for the amount of increase in cluster size. Aggregation plays a dominant role.

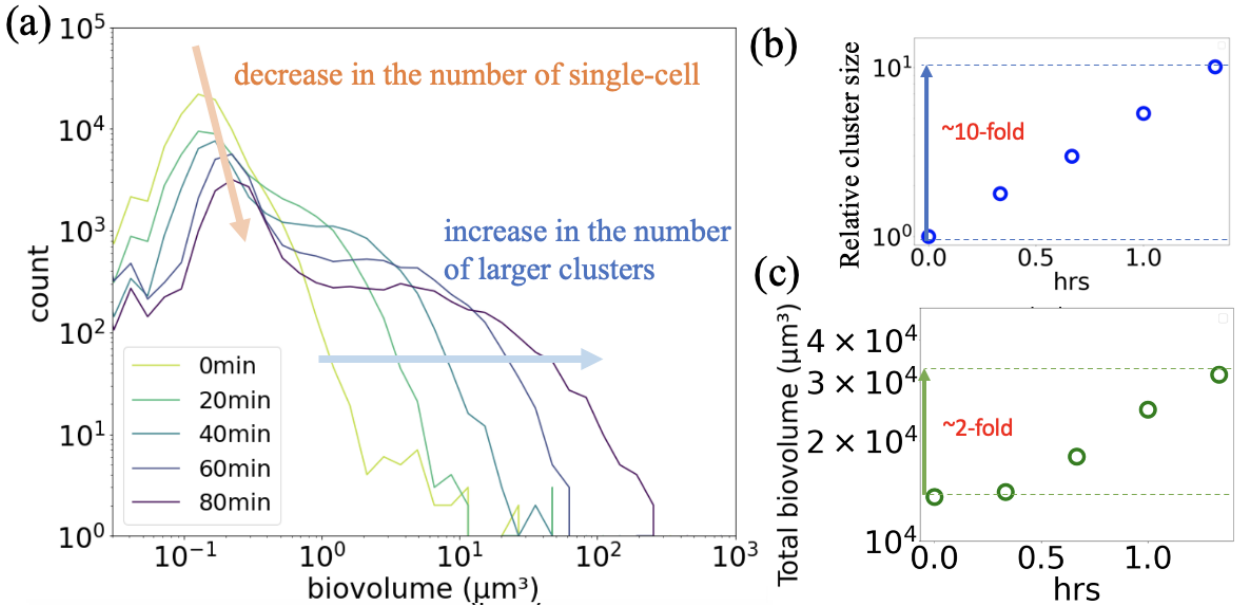

Figure 7. (a) Aggregates size distributions during 80 min after transfer from 40 mM acetate to 0.5% peptone media (b) relative cluster size calculated by total biovolume/number of clusters and then normalize (c) total biovolume vs. time by integrating the size distribution curve

2.2.2 SINGLE CELL DYNAMICS AND MODEL FOR INITIAL PERIOD

As cell growth is small compared to increase in cluster size, we focus on the effect of aggregation and neglect growth as a first approximation. Since the single cell density is significantly larger than the density of larger aggregates in the initial period, we neglect higher order aggregates and further focus on the encounter between single cells and build a model for single cell dynamics.

Assuming β is the encounter rate kernel, from which the encounter rate E can be defined as:

$$E_{ab} = \beta_{ab} \cdot \rho_a \cdot \rho_b \qquad \text{Eq. (1)}$$

where ρ_n is the concentration of n-cell clusters [17].

We assume bacteria swim in straight line and adopt the ballistic encounter kernel [18], in which $\beta_b = A \cdot \Delta v$ (Δv is the relative swimming speed and A is the effective cell cross-section

area). We further assume a stickiness coefficient α, such that the loss term due to single cell sticking into another single cell is

$$\frac{d\rho_1}{dt} = -2E_{11}\alpha = -2 \cdot 2\beta_b\alpha \cdot \rho_1^2 \qquad \text{Eq. (2)}$$

Note that the first 2 on right hand side account for the fact that two single cells are lost when sticking to each other.

Equation 2 can be solved analytically yielding a time-dependent single cell density:

$$\rho_1(0)/\rho_1(t) = 1 + t/\tau \qquad \text{Eq. (3)}$$

where we defined aggregation time τ such that $\tau^{-1} = 4\alpha\beta_{11}\,\rho_1(0) = 2A\Delta v\alpha\rho_1(0)$ is the slope of $\rho_1(0)/\rho_1(t)$ vs. t plot. Here we assume the stickiness and swimming speed is constant over time.

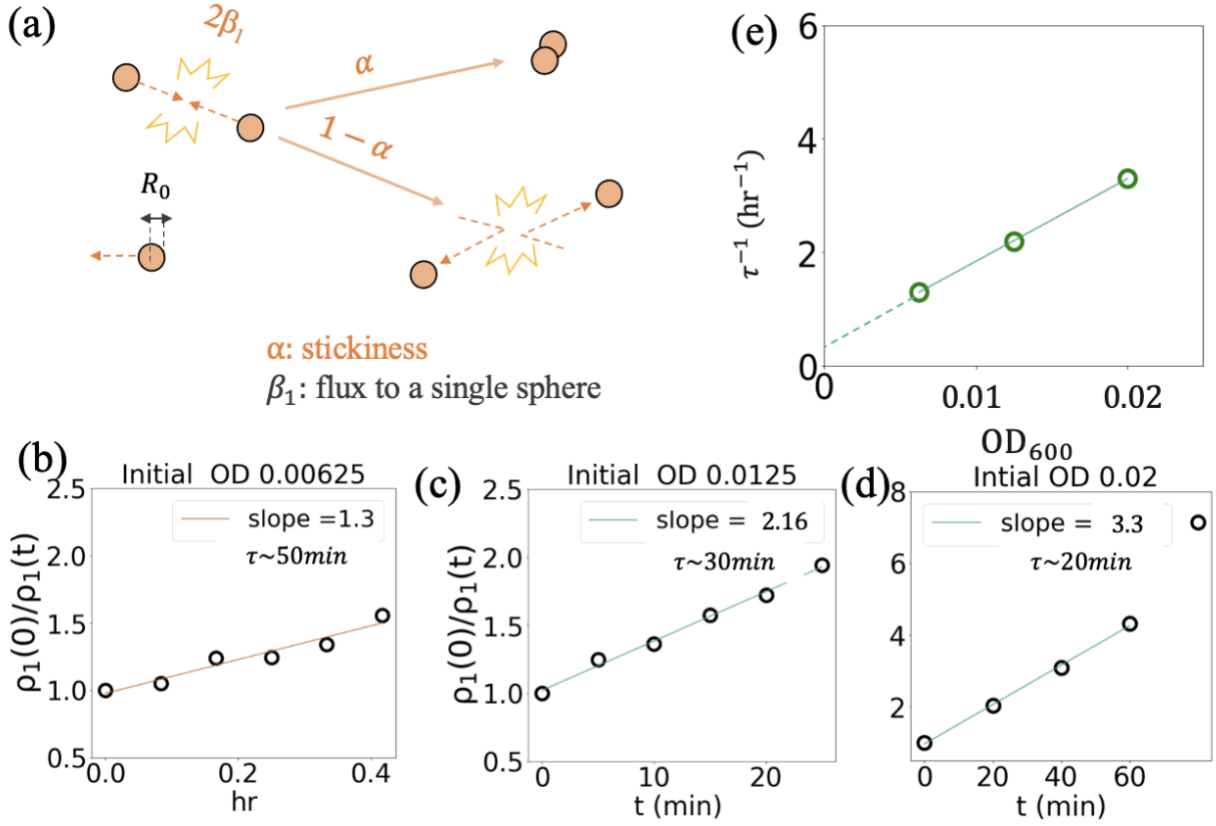

Figure 8. (a) Model for single cell dynamics, (b) (c) and (d) are cell concentrations at 0 min over t min vs. time plot at three different initial OD (e) τ^{-1} extracted from (b), (c) and (d) is plotted with initial OD

To obtain the single cell density through size distribution, we define a single cell region near the single cell peak and integrate the distributions in this region. $\rho_1(0)/\rho_1(t)$ vs. t in peptone 0.5% with three different initial cell density is then plotted. The experiment results are in good agreement with our model by showing a straight line in the plot (Fig. 8 b,c,d). After getting the aggregation time τ under different ODs, and assuming 1OD is 10^9 cells/ml, we are able to extract $\alpha \cdot \Delta v$ by a linear fitting of τ^{-1} and $\rho_1(0)$. If we assume a cell cross section area A ~ $\pi\ \mu m^2$, then $\alpha \cdot \Delta v \sim 3\ \mu m/s$ in peptone 0.5% media. Further motility measurement has been done to determine swimming speed to estimate stickiness.

2.2.3 MOTILITY

To estimate stickiness from aggregation time, we need to measure average swimming speed of 4B03 after being transferred from acetate precultural to peptone batch culture. To better understand the steady state, swimming speed for the trajectory of individual cells from exponential growing peptone and acetate culture were measured. A clear nonmotile peak is observed in acetate culture and motile cells has a wide range of running speed with similar frequency. In peptone culture, it shows a gaussian-like distribution with a peak at around 90 $\mu m/s$. Acetate culture has around half nonmotile cells while almost all cells are motile in peptone culture (Fig. 9). Moreover, the average motile speed is around 1/3 higher in peptone than in acetate. Both results indicate that bacteria have a much higher encounter rate in peptone.

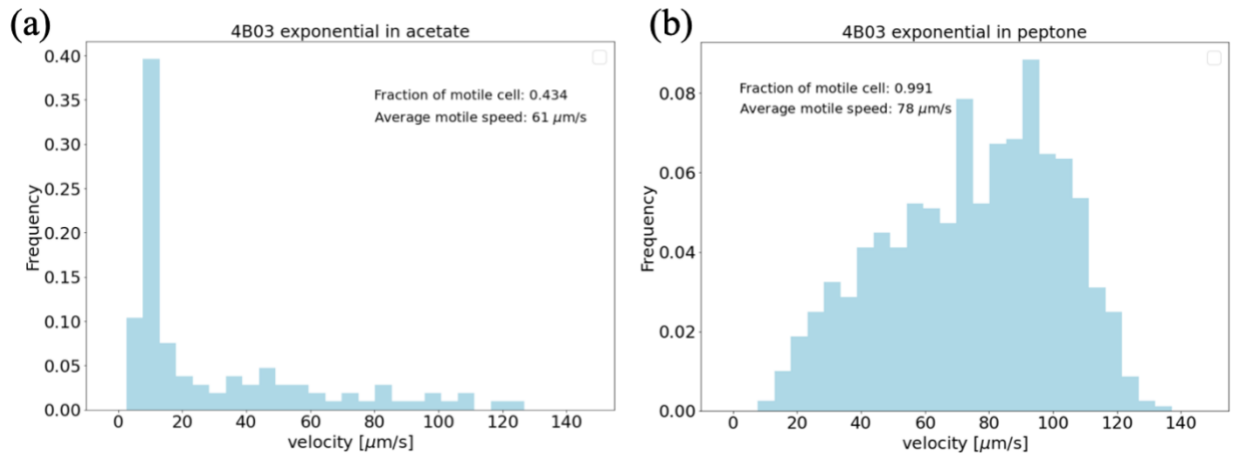

Figure 9. Swimming speed distributions for 4B03 in preculture minimal medium with different carbon source. (a) exponential growth in 40 mM acetate (b) exponential growth in 0.5% peptone. Motile fraction and average motile speed are also obtained from the plot. The motile and nonmotile threshold is set to 20 $\mu m/s$.

Then motility measurement was taken for first 1 h for cells transferred from acetate preculture to peptone culture. A few minutes are needed to sample the culture and adjust microscope, so the first time point measured is around 3-5 min after transfer. Compared with distributions in acetate culture, we see that motile fraction increase dramatically to 0.89 in a few

minutes after being transferred. Average speed for motile cells also increases. The speed distributions for 5 min and 15 min are relatively flat compared to steady state in peptone, suggesting that many cells are running in lower speed and not yet fully adapt to peptone culture. One nonmotile peak and one motile peak can be clearly observed at 30 min and 1 h after transfer. As a result of lower amount of low-speed cells, the average motile speed increases for around 0 μm/s compared to the first 15 min. There are still 10% nonmotile cell 1h after transferred (Figure 10a), indicating that longer time may be needed for cells to fully adapted to peptone and exhibits fully motile (Figure 9b).

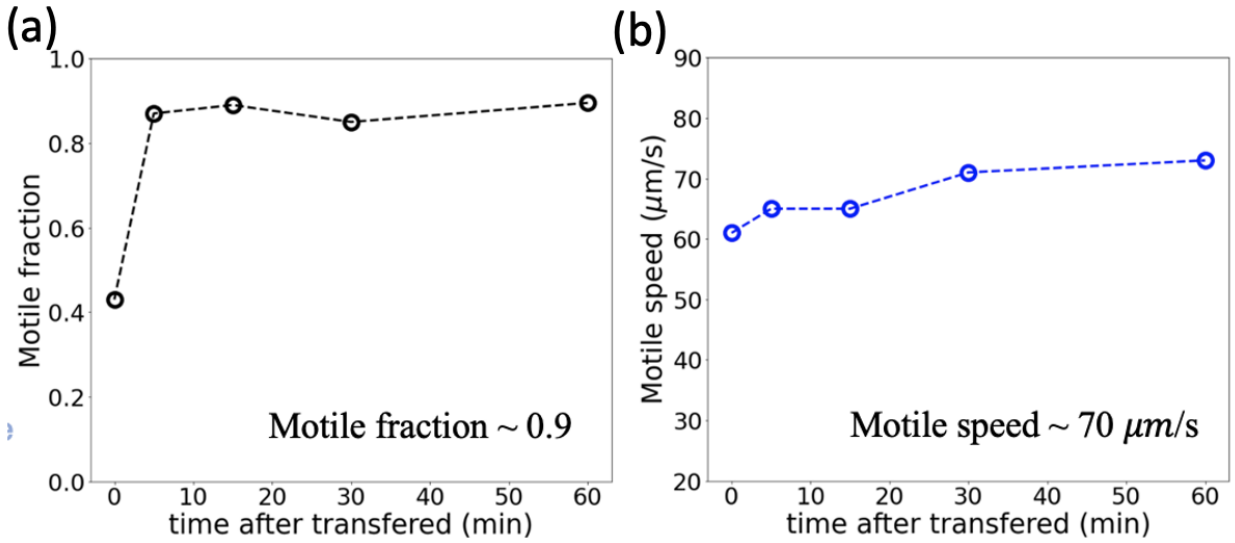

Figure 10. (a) Dynamics motile fraction and (b) motile speed for 4B03 transferred from exponential growth acetate to peptone 0.5%; motility measurements were taken at 0 min, 5 min, 15 min, 30 min and 1 h after transferred; motile and nonmotile threshold is set to 20 μm/s.

Around 90% of single cell is motile in the first hour after transferred according to motility measurements (Fig. 10a). Thus, to estimate the stickiness value, we should refine the model to consider nonmotile single cells. Note that nonmotile single cells can be served as a target for aggregation. The encounter rate kernel of motile-nonmotile cells is half of that of motile-motile cell. Thus, if consider a motile fraction n, the single cell dynamics is:

$$\frac{d\rho_1}{dt} = -2 \cdot 2\beta_b \alpha \cdot n^2 \rho_1^2 - 2 \cdot \beta_b \alpha \cdot n(1-n)\rho_1^2 \quad \text{Eq. (4)}$$

The solution of equation 4 remains the similar form as before:

$$\rho_1(0)/\rho_1(t) = 1 + t/\tau_n \quad \text{Eq. (5)}$$

Here the slop of $\rho_1(0)/\rho_1(t)$ plot $\tau_n^{-1} = 4\alpha\beta_b\,\rho_1(0) \cdot [m^2 + m] = 2\pi R_0^2 v\alpha\rho_1(0) \cdot [m^2 + m]$.

We know that the slop of $\tau_n^{-1}\ vs.\ \rho_1(0)$ is $2\pi R_0^2 v\alpha \cdot [m^2 + m] = 1.5e5\mu m^3/hr$ (Fig. 8). Using an average motile fraction (87%) and an average motile speed (67 μm/s) in first 30 min, we get stickiness $\alpha \sim 0.06$.

2.2.4 TIME-DEPENDENT STICKINESS VALUE

The stickiness value in previous section is the average stickiness in first hour after transfer. Since aggregation rate gradually decrease with time after transferred while motility keeps constant, a changing cell stickiness value might be able to explain the decreasing aggregation. To measure the dynamics cell stickiness, we filtered the culture using 1.5 μm filter at 15min, 30min and 45min after transferred to peptone to get rid of clusters in the culture and leave only single cells (Fig. 11a). Size distributions and thus stickiness was obtained using similar method described before. The stickiness value is above 0.1 right after transfer but drop to half its initial value in 30 min (Fig. 11b). This dynamics single cell stickiness value gives us an idea about how the stickiness effects aggregation.

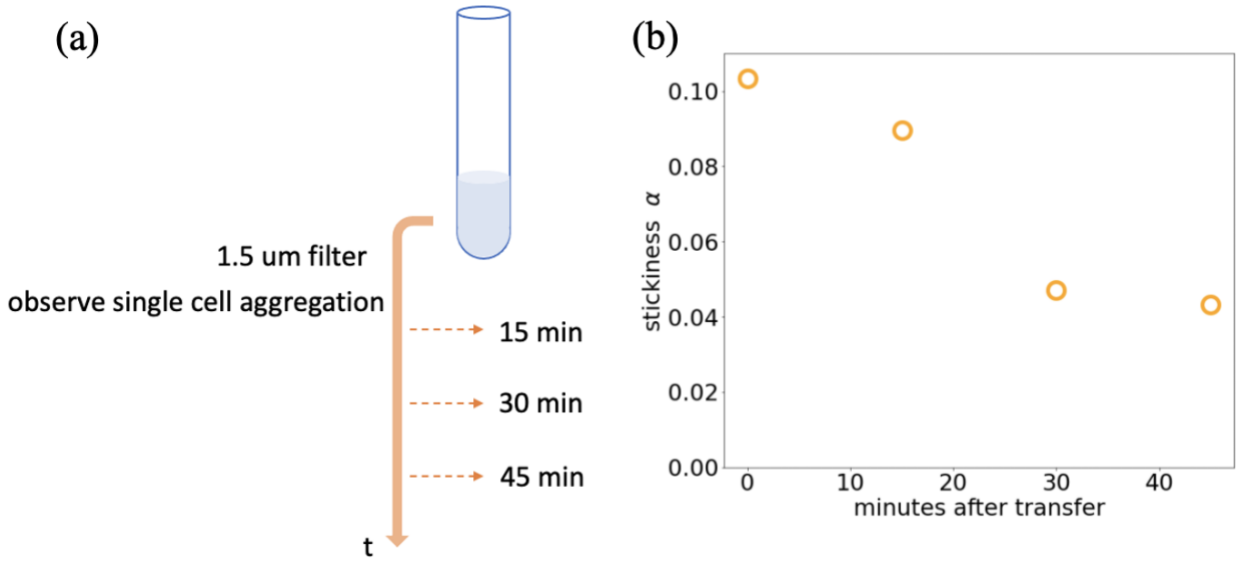

Figure 11. (a) Demonstration of experiment filtered out single cell in different time (b) stickiness values for single cell filtered at different time after transferred (obtained from similar method as before by measuring four time point in 30 min).

2.2.5 SIZE DISTRIBUTIONS IN OTHER NUTRIENT CONDITIONS

Different initial cell density and peptone concentrations were tested before choosing the standard condition (peptone 0.5% and OD ~ 0.2). When peptone concentration is lower than 0.1%, single cell concentration starts to raise up after 50 min and the increase of lager aggregates stopped (Fig. 12). Besides, the decrease in single cell count in the linear range is not as significant as those with higher peptone concentration, resulting in larger measurement error. Peptone 0.25% continues to aggregate in 80 min but the single cell number seems to have two aggregation region with different slope in the inverse singe cell number plot. Thus, for a longer and more steady measurement, we used peptone 0.5% when OD is close to 0.02.

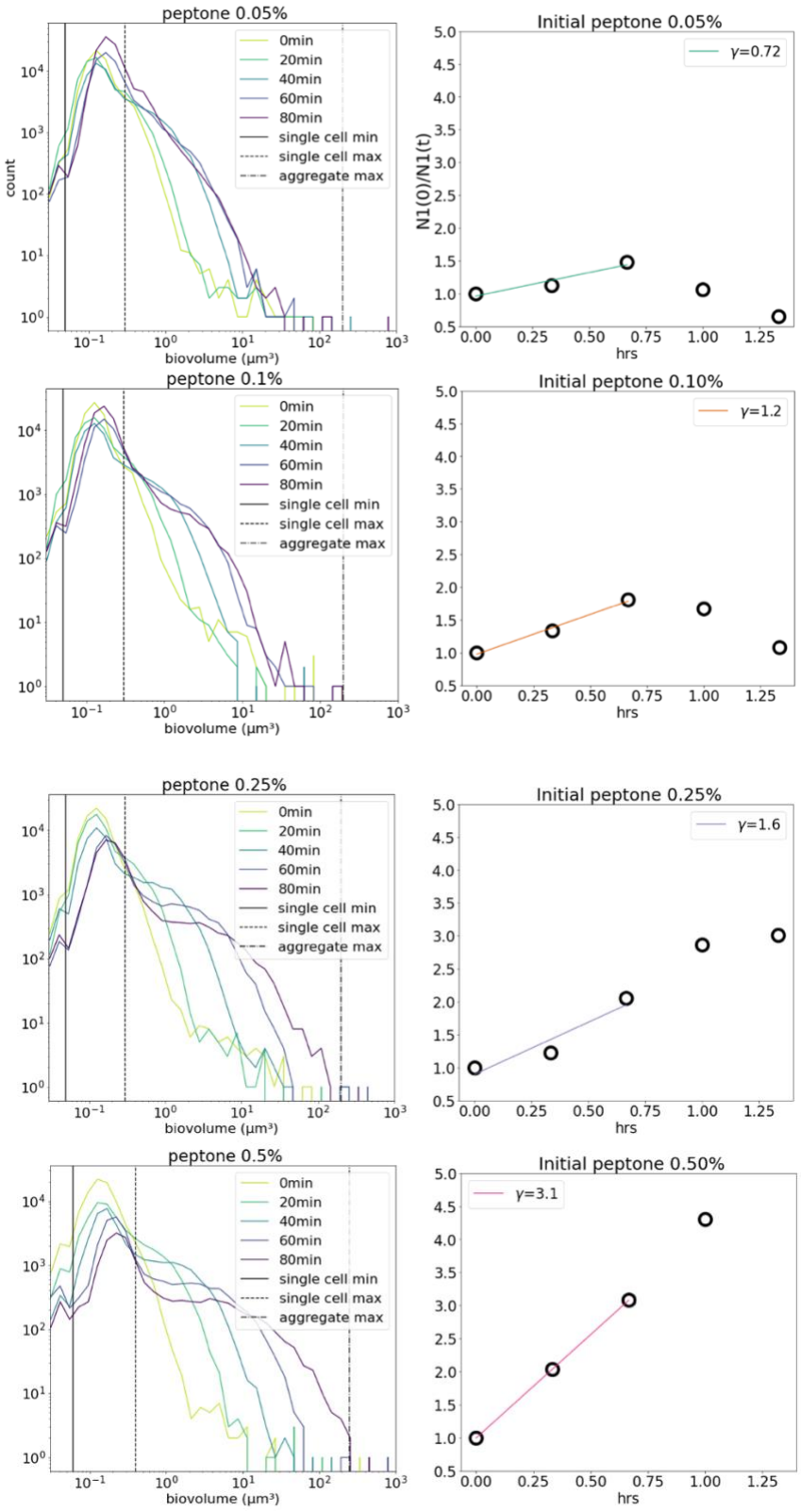

Figure 12. Size distributions and inverse singe cell number plot for four different peptone concentrations with same initial OD 0.02. $\gamma = \tau^{-1}$ is the slope of inverse singe cell count vs. t

Size distributions from higher peptone concentration were also obtained to understand how peptone concentration effect aggregation behaviors. Three different initial cell density with peptone 0.75% was measured for the first 30 min (Fig. 13 a,c). Higher initial cell density results in a faster aggregates formation and faster loss of single cells (Fig. 13 d-f). The inverse aggregation time τ^{-1} increase approximately proportional with initial cell density. With condition OD 0.00625 and peptone 0.75%, the inverse cell count does not follow a straight line but seems to have two aggregation regions. This is similar to what we have observed in OD 0.02 and peptone 0.25%, indicating that the linear region for peptone 0.75% might be in higher cell concentrations. However, the aggregation time, which is the time scale inside which our single cell model would work, is around 15 min for OD 0.025 in peptone 0.75%. Further increase of initial cell density would result in a smaller aggregation time, making it difficult to measure enough time points in the model valid range.

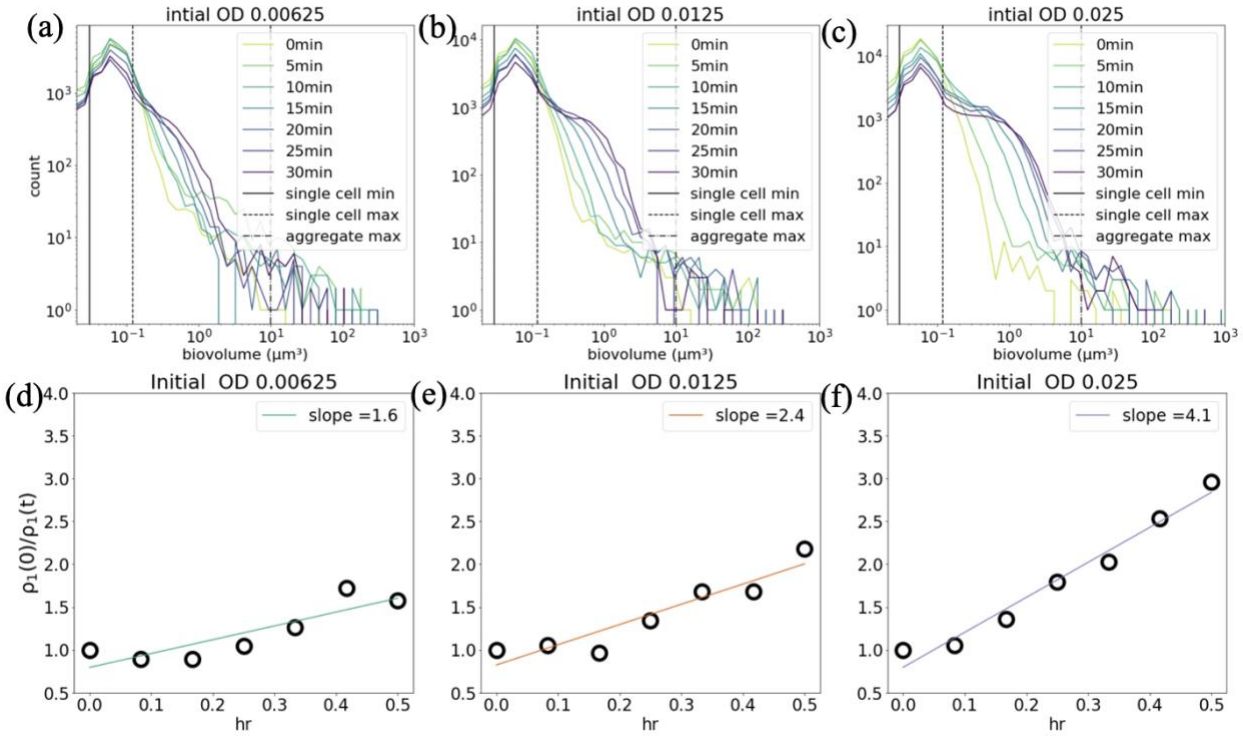

Figure 13. Size distributions and inverse singe cell number plot for initial OD = 0.00625, 0.0125 and 0.025 with same peptone concentration 0.75%

2.2.6 SIMULATIONS

The model above has neglected the effect of clusters contains two or more cells. We want to simulate the system with larger clusters and growth being considered. In this case, the loss term due to cluster-a being absorbed into another cluster is [10]:

$$\frac{d\rho_a}{dt} = -\sum_i \alpha \cdot E_{ai} \qquad \text{Eq. (6)}$$

We denote the growth rate as λ and it is assumed to be constant in time. Other assumptions in these simulations are: 1) cells have a probability q to escape and a probability (1-q) to remain in the cluster when doubling; 2) they do not stick together for single cell doubling (based on microscope observation); 3) Consider only single cells adding to clusters, that is to say, only single is motile. And assume the motile fraction of single cell is n, so the portion of nonmotile single cell is (1-n).

Single cell can be formed by single cell doubling and cells escaping from clusters and can be lost by collision between two motile single cells, one motile cell collide with another nonmotile single cells or with clusters. Thus, the rate of change for single cell population is:

$$\frac{d\rho_1}{dt} = -2 \cdot 2\beta\alpha \cdot \rho_1^2 n^2 - 2\beta\alpha \cdot n\rho_1 \cdot (1-n)\rho_1 - \sum_{i=2}^{N} \beta\alpha \cdot \rho_i \cdot n\rho_1 + \lambda \cdot \rho_1 + \sum_{i=2}^{N} q \cdot \lambda \cdot i \cdot \rho_i$$

Eq. (7)

Here we assume that the radius for n-cell clusters r_n does not change much for different n. In this case $\beta_{11} = \beta_{12} = \beta_{22} = 2\beta, \beta_{1n}(n > 2) = \beta_{2n}(n > 2) = \beta$ and $\beta_{mn}(m > 2, n > 2) = 0$, where $\beta = \pi R_0^2 \cdot v$. A more rigorous assumption would be $r_n \propto n^{1/3}$. N is the largest clusters to be considered.

Two cell clusters can be formed by collision between two motile single cells or between one motile single cell and one nonmotile single cell. It can be lost by cell doubling and aggregate with single cells. Thus, for two cell clusters,

$$\frac{d\rho_2}{dt} = 2\beta\alpha \cdot \rho_1^2 n^2 + \beta\alpha \cdot n\rho_1 \cdot (1-n)\rho_1 - \beta\alpha \cdot n\rho_1 \cdot \rho_2 - 2\lambda(1-q) \cdot \rho_2$$

Eq. (8)

where the $2\lambda(1-q) \cdot \rho_2$ term on right hand side indicates the loss of two cell clusters due to doubling of cells inside cluster. This term would become $n\lambda(1-q) \cdot \rho_n$ for n-cell clusters.

For j-cell clusters (j > 2):

$$\frac{d\rho_j}{dt} = \beta\alpha \cdot n\rho_1 \cdot \rho_{j-1} - \beta\alpha \cdot n\rho_1 \cdot \rho_j - j\lambda(1-q) \cdot \rho_j + \lambda(j-1)(1-q) \cdot \rho_{j-1}$$

Eq. (9)

The above equations were checked by adding up the total number of cells:

$$\frac{dN}{dt} = \frac{d(\sum_n n \cdot \rho_n)}{dt} = \lambda \cdot N \qquad \text{Eq. (10)}$$

Based on experimental measurement for single cell decreasing rate (Fig.8) and growth rate (Fig.1 and Fig.7), $\beta\alpha = 0.375 \cdot 10^5 \mu m^3/hr$ and an average growth rate for the first 1.5h $\lambda = 0.6\ hr^{-1}$ was used in the simulation.

Different escaping probability and motile fractions of single cells were used to understand their effect on aggregation. A larger escaping probability causes a slower aggregation and less decrease in single cell. A higher motile fraction results a faster aggregation and faster decrease in single cell concentration. When the motile fraction reduced to a certain level, single cell concentration increases with time. Possible limitations of this simulation are that we assume a constant motile fraction, motility and stickiness while in reality these parameters could change with time.

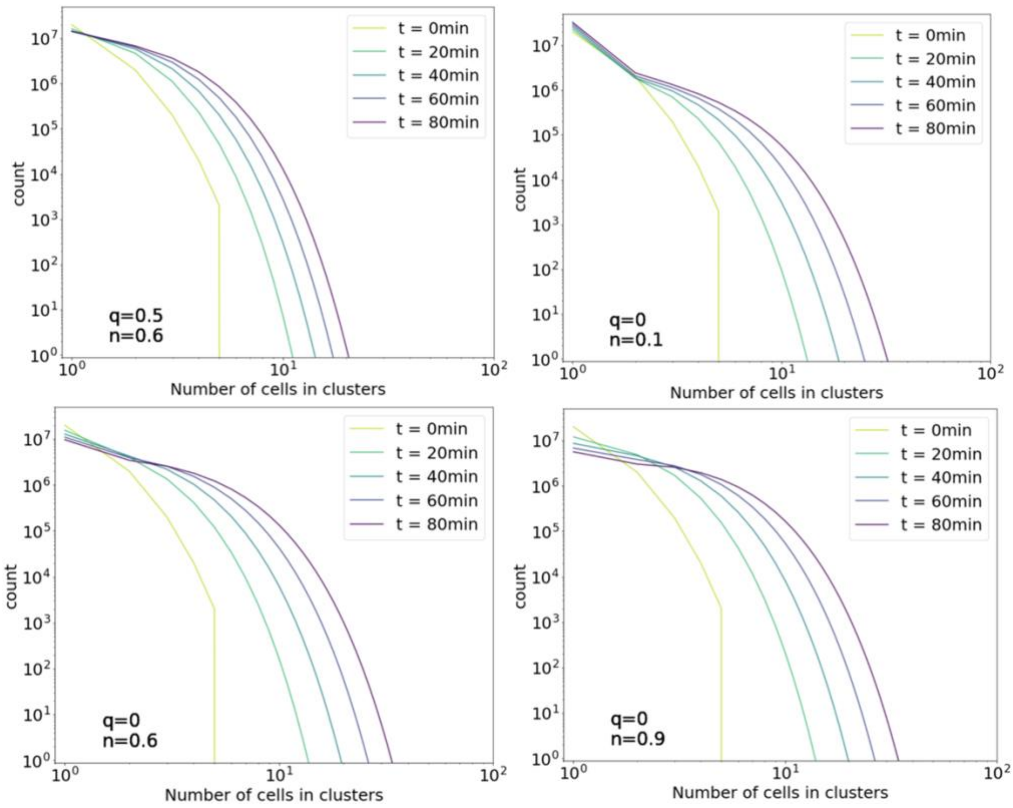

Figure 14. simulated size distributions using various escaping probability q and motile fraction n with growth rate 0.6 hr^{-1}.

Assuming a zero escaping probability and an 100% motile single cells fraction, single cell population decrease for 4-fold in the first 1.5h in simulation (Fig. 15a) which approximately agrees with the experimental data (Fig. 8d). It decreases a little bit more in experiment, indicating that the model might have underestimated single cell aggregation rate. The simulated size distributions were replotted using same axels' scales as in experimental plot (Fig. 15b) for comparation. Experimental distributions (Fig. 7a) expand much more than simulated one. So there is clearly something that promote aggregation that is not taking into account in the simulation. The encounter rate of single cell with larger clusters should increase with increasing cross-section area for larger clusters, which means $\beta = A \cdot \Delta v \sim \pi r^2$ where $r \propto \text{number of cells}^{1/3}$. Simulated size distributions using same parameters but taking changing β value into account is plotted (Fig. 15c). There is much more decreasing in single cell but not much additional expansion in larger clusters.

Then we turned the stickiness value to 1, which means cell immediately stick together upon collision. Single cell count decreases dramatically with time while only a little expansion observed in larger cluster (Fig. 15c).

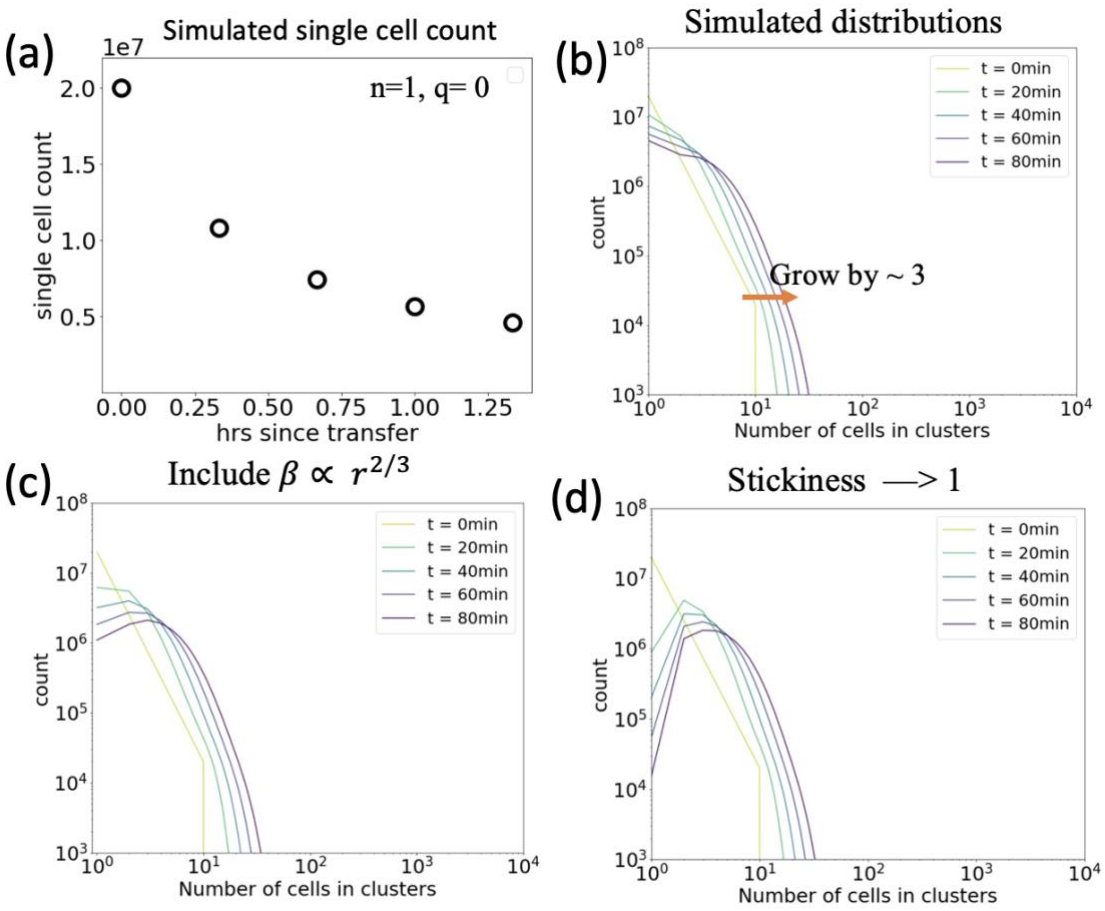

Figure 15. (a) simulated single cell count using an escaping probability q=0 and single cell motile fraction n=1; (b) simulated size distributions using the same parameters as (a); (c) simulated size distributions considering increasing encounter rate with increasing cross-section area; (d) simulated size distributions using the same parameters as (a) but assuming a stickiness value 1.

Our simulation result indicates that while the loss of single cell is dominated by single cell-single cell collision, the picture that considering only single cell adding to cluster could not explain the rapid expansion of biovolume of the clusters. There might be cluster-cluster interactions or chemotaxis attraction from clusters that promote aggregation to clusters. Further theoretical work could be done to investigate in this topic.

2.3 EXPERIMENTAL METHODS

2.3.1 EXPERIMENTAL SETUP

Single colony of Alteromonas sp. 4B03 was picked from an MB agar plate and transferred into 16ml tube containing 2 ml Marine Broth. P1000 filter tip was used here to pick colony and resuspend in MB media. The tube was then incubated in 27°C shaker for around 4-12 hours which serve as the seed culture. The seed culture was centrifuged and wash and resuspend in 1.5 ml centrifuge tube with preculture minimal medium [19] with 40mM HEPES pH 8.2 and 4 mM Tricine pH 7.4 as buffer. Cells were then diluted in preculture medium with 40 mM Na-acetate added and incubated in 27°C shaker overnight to grow to high density culture OD 0.5-1.0 by experiment time. The importance of the preculture is to give cells time to adjust their physiology for the experimental conditions. Before experiment start, OD of precultures were taken to confirm that cells are in exponential growth state. Centrifuge precultures for 120 seconds at 9,200 rpm in 1.5 ml centrifuge tube, wash and resuspend cells in batch culture media with no carbon source (same recipe with preculture medium except instead of using HEPES buffer we used 2 mM Sodium Bicarbonate). Then the culture was filtered using 1.5 um filter and 1 ml syringe to enrich single planktonic cells. Filtered cells were inoculated into 8 ml prewarmed fresh batch culture medium in 25 ml tube and cultured in 27°C water bath. For OD-based measurement, tubes were put in 27°C shaker for a measurable aggregation fraction. For chamber measurement by confocal microscope, tubes were kept static in water bath for a more precise measurement of aggregates' size distributions over time.

2.3.2 SAMPLE PREPARATION FOR MICROSCOPY

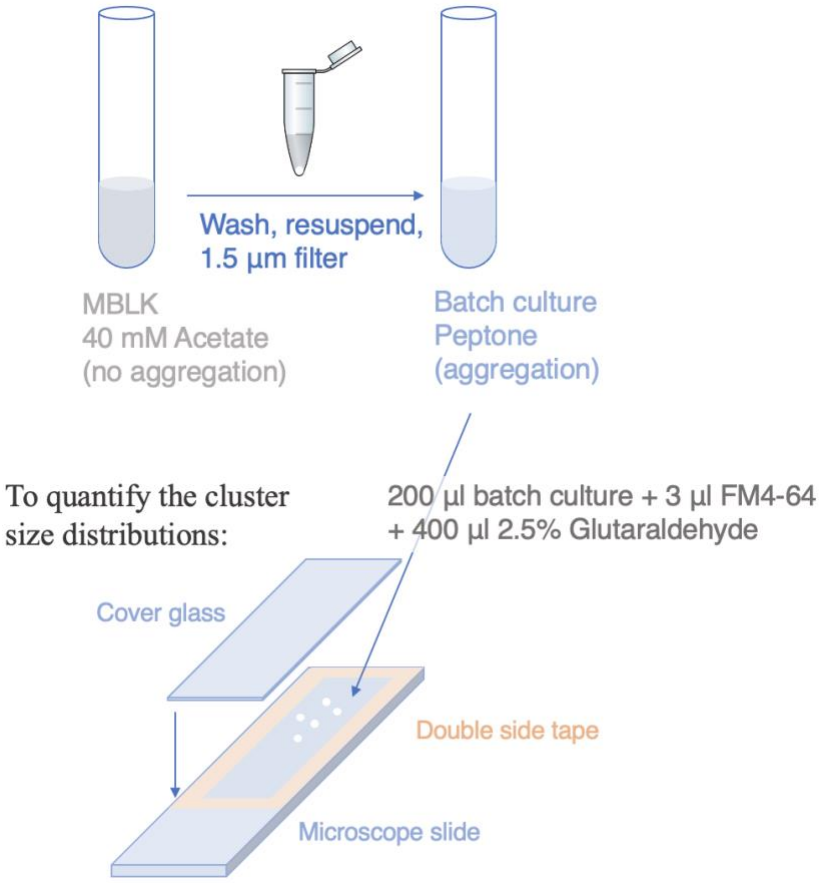

Figure 16. Schematic chamber loading process and transferring cells from acetate preculture to peptone batch culture.

At every timepoint for each tube, 200 µl culture was sampled and put in a 1.5 ml black tube with 3 µl FM 4-64FX dye already added inside. Then, 400 µl of 2.5% glutaraldehyde in PBS was immediately added to the black tube to fix cells. We gently inverted black tubes for several times to better mix the dye and fixatives with cells. For experiments with denser timepoints and short timescale (such as sample every 5 min for 30 min), the fixed cells were loaded into chamber at the end of the experiments. For longer timescale experiments, the chambers were loaded right after each timepoints.

Chamber loading: we first attached a rectangular cut-out adhesive transfer tape (3M 468MP) to 25x75mm microscope slides (VWR 48312-004) for each tube/chamber to be loaded. Suspend dyed and fixed culture by gently inverting black tubes for three times, then take 90 μl from this tube into the half-made chamber. Deposit cell suspension toward one end of the chamber. Starting at the same end of the chamber, carefully place a 25x50mm cover glass (VWR 10118-789) to seal the chamber (Fig. 16). To achieve an even seal with minimal bubbles, this is done slowly in a reverse peeling motion. Then, we flip over loaded chambers so that cells sink onto cover glass. Chambers were rest overnight to achieve full settling, covered in foil to protect the dye from bleaching.

2.3.3 FLORESCENCE CONFOCAL MICROSCOPY AND IMAGE ANALYSIS

The chamber was then measured using a Leica confocal microscope controlled by LAS AF. We use Fluorescence SpectraViewer to determine the compatible laser and the range of detector wavelength. The fluorescence excitation/emission (Ex/Em) wavelength of FM 4-64FX is 505nm/726nm. Two lasers (488 nm, laser power 2% and 552 nm, laser power 5%) were applied and a detector range of 650-750 nm was used. We confirmed before imaging that cells/clusters were all in the bottom. For each chamber, the image was obtained by tile scanning in the x-y plane for an area around 0.5cm x 1cm and then merge into a single image. 10x objective was used for chamber scanning. The resolution of each image is 512x512 with 489.24 nm^2 pixel size under zoom factor 4.0.

Images were analysis using python scikit-image. The original image was converted to float, gaussian filtered with σ between 0.4 to 1 to smooth the background noise while keeping single cells clear, then small objects (< 2 to 5 pixel squared) was removed to reduce the chance of any

background to be counted as cells. With the last processed image, a histogram of particle size distribution was obtained (Fig. 17).

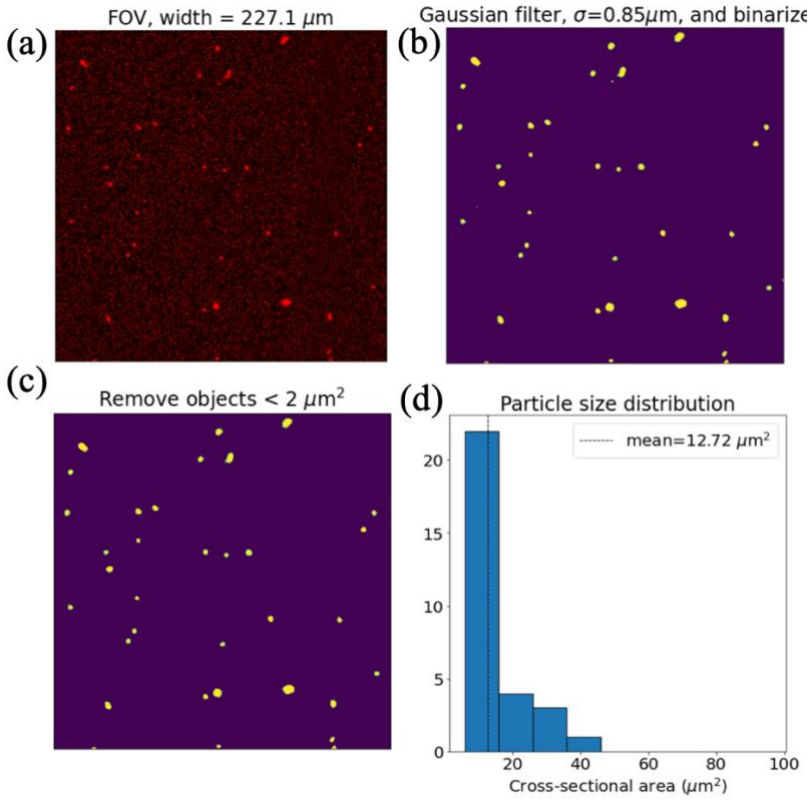

Figure 17. Image analysis in Python: (a) original image (b) image after gaussian filter with σ = 0.85 (c) image after removing small objects (d) histogram

2.3.4 BIOVOLUME STANDARD CURVE

Since the histogram we get in last section was the cross-section histogram, we want to get the biovolume distributions to have a better understanding of the aggregation dynamics. To do that, same aggregate was imaged under 10x objective to get cross-section area and used z-stack image under 40x objective to get its biovolume. The 10x image was taken under zoom 4.0 as our standard setting. Several aggregates with various sizes were measured this way and then we can obtain a biovolume vs. cross section curve (Fig.18c). Here biovolume = 0.0081(cross-section area)$^{1.4}$. Note

that the power is close to 1.5 which we would expect. We are then able to convert the measured cross-section to its corresponding biovolume using this relationship.

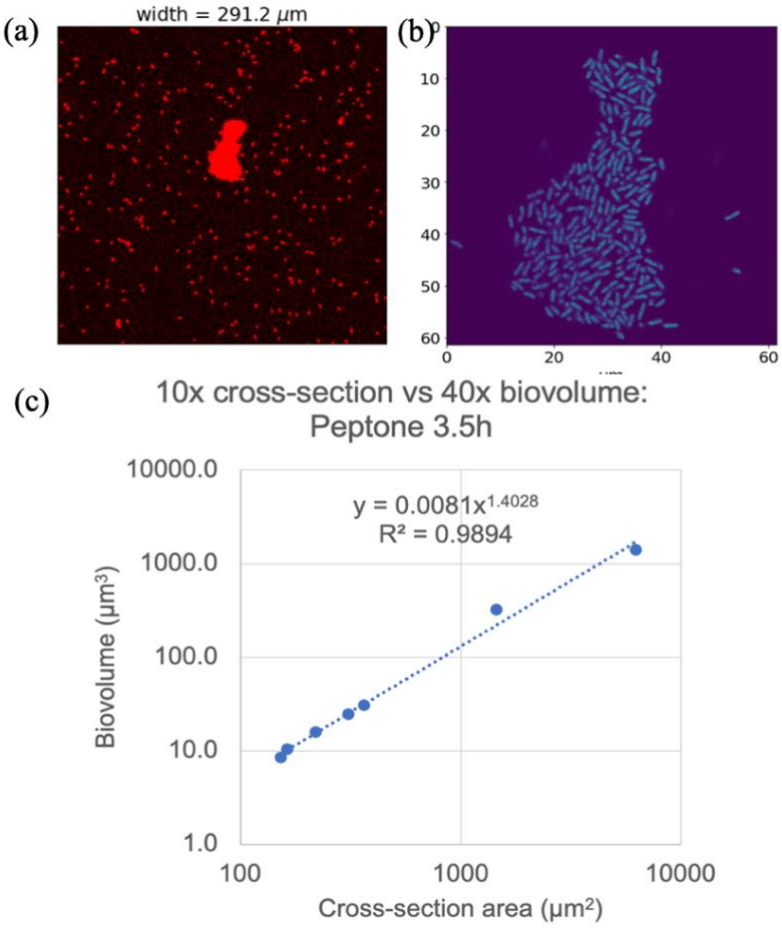

Figure 18. (a) Aggregate under 10x objective, (b) the same aggregates under 40x objective, (c) biovolume vs. cross-section area curve. Each point represents an aggregate (credit: Jacob Robertson)

2.3.5 MOTILITY MEASUREMENT AND CELL TRACKING

Motility was measured using Nikon microscope with a high-speed camera (40 frames per second), controlled by NIS-Elements AR. The video is recorded by uEye-Cockpit. The seed culture and preculture conditions are the same with as mentioned in previous section. Cells from precultures were centrifuged for 120 seconds at 9000 rpm and then transfer into preheated 27 C medium with HEPES as PH buffer to prevent cells from aggregating. Moreover, 0.05% PVP40

(Polyvinylpyrrolidone) is added in the medium to prevent cells sticking to the glass capillary. We make sure the experimental culture has OD range from 0.005 to 0.01. Then a glass capillary (rectangular 0.4mm x 0.4mm glass capillary) is used to sample the cells and put it under the microscope. Video was recorded for more than 100 second using 10x objective (microns per pixel= 0.468296, depth of field = 9 μm) with a focus set to the middle of the glass capillary. First 1000 frames (25seconds) with HD resolution video (1280x720 pixels) were analyzed.

The detection of cells in each recorded image is done by the built-in functions inside Python packages trackpy and skimage. We first input an estimate size of the cells in pixels and reduce the noise by adding a threshold of total brightness and a minimum signal of the particles. The trajectories are formed by calculating the displacement between the cells of each consecutive frame, where the closest two cells are accepted as the same cell displaced to the next frame. A maximum displacement of cells between each frame is set to 10 pixels (~ 190 μm/s) and we allow cells to be missed for a few frames (5 frames = 0.125s). Moreover, spurious trajectories are filtered out by keeping only trajectories that last longer than 20 frames (0.5s). This is done for all the frames, hence giving a trajectory for each detected cell. Each trajectory is analyzed after averaging over 0.5s intervals (Fig. 19 d). Then, the average swimming speed of each trajectory were calculated and plotted as histogram (Fig. 19 e).

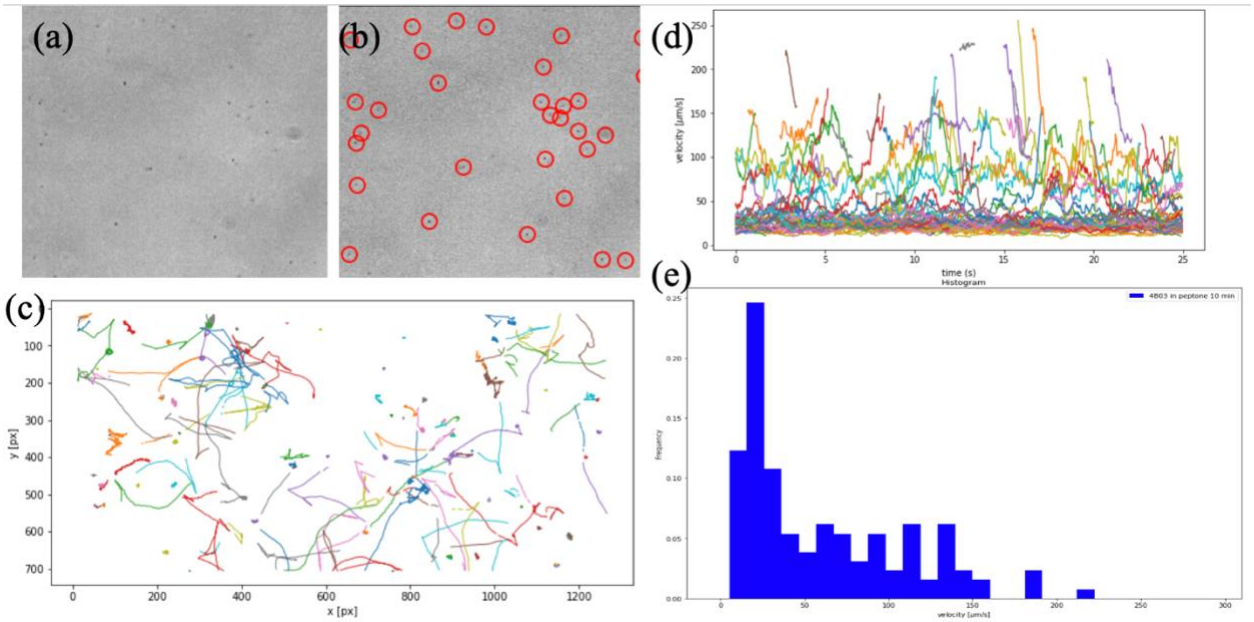

Figure 19. Analysis of exponentially growing 4B03 after transfer from acetate to peptone for 10 min. (a) original image (b) cell detection for the same image (c) trajectories of cells in 1000 frames (d) instant velocity vs. time of each detected particle (e) histogram of velocity

Acknowledgements

Chapter 2 in part is currently being prepared for submission for publication of the material. Robertson, Jacob; Wu, Yonghan; Hwa, Terence “Microscopic size distributions and coagulation modeling allow estimation of cellular stickiness in copiotrophic marine bacterium Alteromonas sp. 4B03". The thesis author was the primary researcher and author of this chapter.

3. CONCLUSION AND OUTLOOK

A nutrient-dependent aggregation behaviors have been found in Alteromonas sp. 4B03. Specifically, they exhibit rapid aggregation and fast growth rate when transferred from acetate minimal media to peptide-containing media such as peptone, tryptone, or marine broth. Aggregation dynamics in peptone was detailed characterized by obtaining size distributions over time. Using a single cell dynamics model, size distributions, and cell motility measurement, we can estimate cellular stickiness value, which is valuable in physical oceanographic models of particle aggregation. For each nutrient condition, stickiness value and motility may be different and thus the model work in different time range (linear range). Similar method could also be used to explore cell stickiness and aggregation process in different nutrient, temperature conditions, or with other particle-associated strains. The microscopy method to measure single cell losing also enable us to quantify the attachment and detachment rate for particle-colonizing marine bacteria. In all, this method and model provide us with a better understanding in dynamics of bacteria aggregation.

REFERENCES

[1] S. Basu and K. R. M. Mackey, *Phytoplankton as Key Mediators of the Biological Carbon Pump: Their Responses to a Changing Climate*, Sustainability (Switzerland) **10**, (2018).

[2] F. Azam and F. Malfatti, *Microbial Structuring of Marine Ecosystems*, Nature Reviews Microbiology **5**, 782 (2007).

[3] J. T. Turner, *Zooplankton Fecal Pellets, Marine Snow, Phytodetritus and the Ocean's Biological Pump*, Progress in Oceanography **130**, 205 (2015).

[4] E. Kaltenbock and G. J. Herndl, *Ecology of Amorphous Aggregations (Marine Snow) in the Northern Adriatic Sea. IV. Dissolved Nutrients and the Autotrophic Community Associated with Marine Snow*, Marine Ecology Progress Series **87**, 147 (1992).

[5] T. Kiørboe, K. P. Andersen, and H. G. Dam, *Coagulation Efficiency and Aggregate Formation in Marine Phytoplankton*, Marine Biology **107**, 235 (1990).

[6] T. Kiorboe, C. Lundsgaard, M. Olesen, and J. L. S. Hansen, *Aggregation and Sedimentation Processes during a Spring Phytoplankton Bloom: A Field Experiment to Test Coagulation Theory*, J.Mar.Res. **52**, 297 (1994).

[7] H. P. Grossart, T. Kiørboe, K. W. Tang, M. Allgaier, E. M. Yam, and H. Ploug, *Interactions between Marine Snow and Heterotrophic Bacteria: Aggregate Formation and Microbial Dynamics*, Aquatic Microbial Ecology **42**, 19 (2006).

[8] H. Ploug, H. P. Grossart, F. Azam, and B. B. Jørgensen, *Photosynthesis, Respiration, and Carbon Turnover in Sinking Marine Snow from Surface Waters of Southern California Bight: Implications for the Carbon Cycle in the Ocean*, Marine Ecology Progress Series **179**, 1 (1999).

[9] A. Gärdes, M. H. Iversen, H. P. Grossart, U. Passow, and M. S. Ullrich, *Diatom-Associated Bacteria Are Required for Aggregation of Thalassiosira Weissflogii*, ISME Journal **5**, 436 (2011).

[10] T. Kiørboe, H. P. Grossart, H. Ploug, and K. Tang, *Mechanisms and Rates of Colonisation of Sinking Aggregates*, Applied and Environmental Microbiology **68**, 3996 (2002).

[11] H. P. Grossart, K. W. Tang, T. Kiørboe, and H. Ploug, *Comparison of Cell-Specific Activity between Free-Living and Attached Bacteria Using Isolates and Natural Assemblages*, FEMS Microbiology Letters **266**, 194 (2007).

[12] M. S. Datta, E. Sliwerska, J. Gore, M. F. Polz, and O. X. Cordero, *Microbial Interactions Lead to Rapid Micro-Scale Successions on Model Marine Particles*, Nature Communications **7**, (2016).

[13] E. F. DeLong, D. G. Franks, and A. L. Alldredge, *Phylogenetic Diversity of Aggregate-attached vs. Free-living Marine Bacterial Assemblages*, Limnology and Oceanography **38**, 924 (1993).

[14] S. Thiele, B. M. Fuchs, R. Amann, and M. H. Iversen, *Colonization in the Photic Zone and Subsequent Changes during Sinking Determine Bacterial Community Composition in Marine Snow*, Applied and Environmental Microbiology **81**, 1463 (2015).

[15] S. G. Acinas, J. Antón, and F. Rodríguez-Valera, *Diversity of Free-Living and Attached Bacteria in Offshore Western Mediterranean Waters as Depicted by Analysis of Genes Encoding 16S RRNA*, Applied and Environmental Microbiology **65**, 514 (1999).

[16] C. L. Dupont, J. P. McCrow, R. Valas, A. Moustafa, N. Walworth, U. Goodenough, R. Roth, S. L. Hogle, J. Bai1, Z. I. Johnson, E. Mann, B. Palenik, K. A. Barbeau, J. C. Venter and A. E. Allen, *Genomes and Gene Expression across Light and Productivity Gradients in Eastern Subtropical Pacific Microbial Communities*, ISME Journal **9**, 1076 (2015).

[17] T. Kiørboe, *Small-Scale Turbulence, Marine Snow Formation, and Planktivorous Feeding*, Scientia Marina **61**, 141 (1997).

[18] A. W. Visser and T. Kiørboe, *Plankton Motility Patterns and Encounter Rates*, Oecologia **148**, 538 (2006).

[19] K. Amarnath, A. v. Narla, S. Pontrelli, J. Dong, T. Caglar, B. R. Taylor, J. Schwartzman, U. Sauer, O. X. Cordero, and T. Hwa, *Stress-Induced Cross-Feeding of Internal Metabolites Provides a Dynamic Mechanism of Microbial Cooperation*, BioRxiv 2021.06.24.449802 (2021).